

Precious-Metal-Free Nanocatalysts for Highly Efficient Hydrogen Production from Hydrous Hydrazine

Jun Wang, Yang Li, and Yu Zhang*

Hydrous hydrazine ($\text{H}_2\text{NNH}_2\cdot\text{H}_2\text{O}$) has generally been considered a promising hydrogen storage carrier because of inherent advantages such as its high hydrogen content and easy recharging as a liquid. Unfortunately, the decomposition of hydrous hydrazine to H_2 is terribly sluggish and/or not entirely favored—a competing decomposition to ammonia may be preferred. This has been the case using noble-metal catalysts and using non-precious-metal-based catalysts, even at elevated temperatures. To overcome this challenge, non-precious-metal-based $\text{Cu}@\text{Fe}_5\text{Ni}_5$ core@shell nanocatalysts are prepared using an in situ seeding-growth approach. Unexpectedly, the catalyst exerts 100% H_2 selectivity and excellent activity and stability toward the complete decomposition of hydrous hydrazine, which is due to the synergistic effect of the core@shell structure. These promising results will certainly promote the effective application of hydrous hydrazine as a potential hydrogen storage material.

1. Introduction

Hydrogen is generally proposed to be an important energy vector for facing the ever-increasing levels of the energy crisis and of environmental pollution due to its high energy density and efficiency with low environmental load.^[1,2] However, even after several decades of intensive exploration, hydrogen storage is still one of the most challenging barriers that impede the implementation of the hydrogen-based economy.^[2] Hydrous hydrazine ($\text{N}_2\text{H}_4\cdot\text{H}_2\text{O}$) is considered a promising liquid-hydrogen storage material due to its high content of hydrogen (8.0 wt%) and its ability for CO-free H_2 production.^[3] Hydrazine is usually used as a propellant for some special applications, such as unmanned space vehicles and submarine power sources.^[4] However, to maximize the efficacy of hydrazine as a hydrogen storage material, one must follow the desired reaction pathway: $\text{H}_2\text{NNH}_2 \rightarrow \text{N}_2 + 2\text{H}_2$, and avoid the unwanted

ammonia-producing reaction: $3\text{H}_2\text{NNH}_2 \rightarrow 4\text{NH}_3 + \text{N}_2$.^[5] The development of highly H_2 -selective (as opposed to NH_3 -selective) and highly efficient catalysts, especially based on non-precious and abundant metals, is of crucial importance for the effective application of hydrazine.

To this end, Xu and co-workers developed a series of bimetallic nanocatalysts (NCs) by alloying Ni with another noble metal, such as Rh, Pt and Ir,^[6] 100% H_2 selectivity (i.e., over the ammonia-producing decomposition) has already been successfully achieved. Thereafter, our group further improved the reaction kinetics via a synergistic effect of the graphene support, the RhNi nanoparticles (NPs), and the use of NaOH.^[7] Nevertheless, the incorporation of noble metals to

nickel greatly increases the cost of catalysts. In a subsequent study, Xu and co-workers synthesized FeNi alloy NCs for their complete and hydrogen-selective decomposition of $\text{N}_2\text{H}_4\cdot\text{H}_2\text{O}$ in the presence of NaOH at 70 °C.^[8] In addition, very recently highly dispersed Ni/ Al_2O_3 NCs derived from Ni-Al hydrotalcite reported by Zhang and co-workers revealed 93% H_2 selectivity for the catalytic decomposition of $\text{N}_2\text{H}_4\cdot\text{H}_2\text{O}$ at 30 °C.^[9] Although these encouraging results have been achieved, the improvements are still far from satisfying. For example, the catalytic kinetics of the FeNi alloy NCs is still terribly sluggish even at a relatively high reaction temperature. As for the Ni/ Al_2O_3 NCs, the small amount of impurity (NH_3) not only reduces the yield of H_2 , but it also poisons current fuel-cell devices, thus requiring a sophisticated post-treatment for separation. Consequently, the development of highly hydrogen-selective and efficient precious-metal-free catalysts in order to significantly enhance the kinetic properties under mild conditions remains challenging, but it is crucial for promoting the application of hydrous hydrazine as a hydrogen storage material.

Herein, the successful synthesis of core@shell NCs ($\text{Cu}@\text{Fe}_5\text{Ni}_5$), which do not contain any precious metals, is reported. They exhibit 100% H_2 selectivity and high activity for the complete decomposition of $\text{N}_2\text{H}_4\cdot\text{H}_2\text{O}$ under ambient conditions, which is due to the electronic coupling between the core and shell metals.^[10] Moreover, in light of this synergistic structural and electronic effect, much higher catalytic efficiency can be obtained by replacing Cu with a noble metal for the core. The use of core can significantly reduce the limitations involving reaction temperature for the complete conversion of $\text{N}_2\text{H}_4\cdot\text{H}_2\text{O}$ to H_2 .

J. Wang
University of Chinese Academy of Sciences
Beijing 100049, P. R. China

Y. Li, Prof. Y. Zhang
Key Laboratory of Bio-inspired Smart Interfacial Science
and Technology of Ministry of Education
School of Chemistry and Environment
Beihang University
Beijing, 100191, P. R. China
E-mail: jade@buaa.edu.cn



DOI: 10.1002/adfm.201401731

2. Results and Discussion

The synthesis of Cu@Fe₅Ni₅ NCs follows an in-situ seeding-growth approach as reported previously.^[11] Briefly, the whole synthetic process can be achieved simply by introducing ammonia borane (NH₃BH₃), as a weak reducing agent, into an aqueous solution containing Cu(NO₃)₂, FeSO₄, and NiCl₂ with a molar ratio of 0.02:0.1:0.1 in the presence of polyvinylpyrrolidone (PVP) as a capping agent. The core Cu NPs are able to form first due to the high reduction potential of Cu²⁺. Subsequently, the in-situ generated Cu NPs catalytically reduce Fe²⁺ and Ni²⁺, which cannot be directly reduced by NH₃BH₃. As a result, the successive growth of Fe and Ni on the surface of the Cu NPs leads to the formation of Cu@Fe₅Ni₅ core@shell NPs. The formation process is observable by the gradual color evolution of the solution (see Supporting Information (SI): Figure S1). In order to reveal the improved catalytic activity derived from the synergistic effect of the core@shell structure for N₂H₄·H₂O dehydrogenation, CuFe₅Ni₅ alloy NCs were also prepared for comparison using a relatively stronger reducing agent (NaBH₄).

Transmission electron microscopy (TEM) was used to characterize the two as-prepared NCs, and the images confirm the success in obtaining the core@shell nanostructure via the in-situ seeding-growth approach. The two NCs are both composed of aggregated NPs with roughly spherical shape (SI: Figure S2a,b). Statistical analyses based on 100 NPs revealed that the average

particle sizes of Cu@Fe₅Ni₅ and CuFe₅Ni₅ are ≈8.5 and ≈7.6 nm, respectively (SI: Figure S2c,d). The TEM image of Cu@Fe₅Ni₅ NPs (Figure 1a) clearly reveals that a distinct contrast between the core and shell sections can be observed. The high-resolution TEM (HRTEM) image (Figure 1b) shows that the core is in crystalline state with a *d* spacing of 0.209 nm, which can be assigned to the {111} plane of Cu. Meanwhile, no lattice fringes are observed in the shell, indicating its amorphous state. These are also consistent with the corresponding selected-area electron diffraction (SAED) patterns (Figure 1b inset), in which the crystalline nature of metallic Cu is revealed. The energy dispersive spectroscopy (EDS) profile (Figure 1c) illustrates the presence of Cu, Fe, and Ni with an atomic ratio of 9.57:44.53:45.90, which was also confirmed by inductively coupled plasma atomic emission spectroscopy (ICP-AES; 1:4.76:4.83), corresponding to the specified atomic ratio and indirectly confirming that both Fe²⁺ and Ni²⁺ can be catalytically reduced by Cu NPs with NH₃BH₃ to form the FeNi shell. We then analyzed the X-ray diffraction pattern (XRD) of the Cu@Fe₅Ni₅ NCs (Figure 1d). The prominent diffraction peaks with the 2θ values of 43.29°, 50.43°, and 74.13° can be indexed to diffractions of the (111), (200), and (220) planes of Cu, respectively (powder diffraction file, PDF #04-0836). Diffraction peaks of Fe or Ni were not present, indicating the amorphous state of the FeNi shell, which is consistent with the results obtained from HRTEM. In contrast, changing the reducing agent (NH₃BH₃) to conventional NaBH₄ resulted only

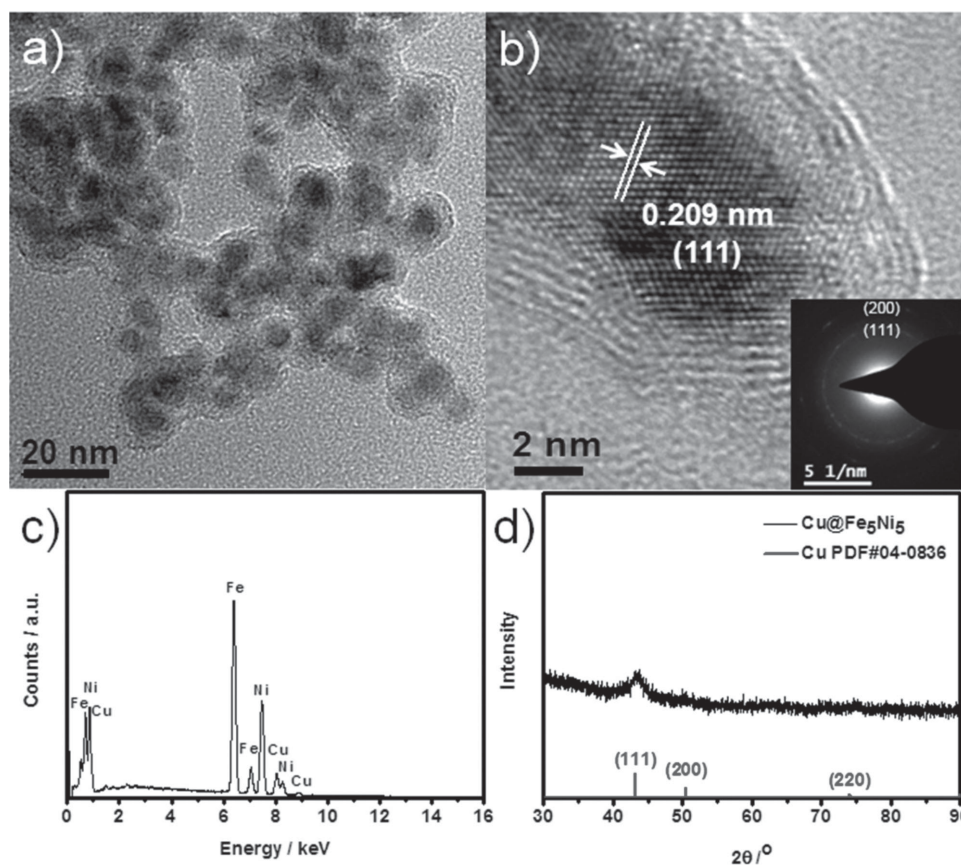


Figure 1. a) TEM image, b) HRTEM image (inset: SAED pattern), c) EDS profile, and d) XRD pattern of as-synthesized Cu@Fe₅Ni₅ NCs.

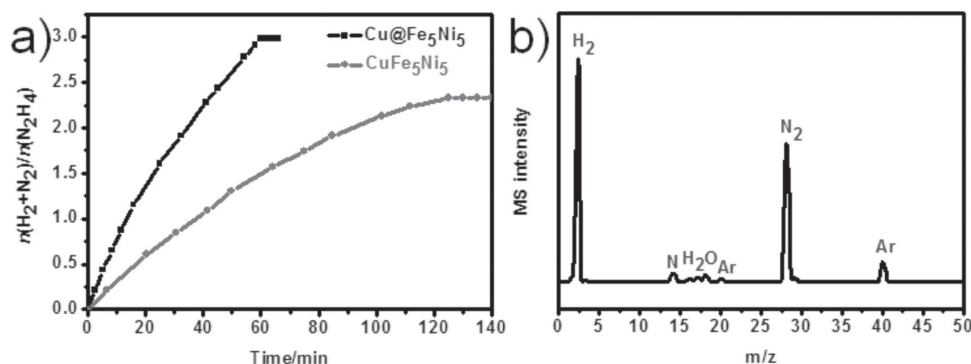


Figure 2. a) Time-course plots for the decomposition of $\text{N}_2\text{H}_4\cdot\text{H}_2\text{O}$ toward H_2 over the $\text{Cu}@Fe_5Ni_5$ and CuFe_5Ni_5 NCs in the presence of NaOH at 70°C ; n represents the number of moles, so $n(\text{H}_2 + \text{N}_2)/n(\text{N}_2\text{H}_4)$ is the ratio of the moles of the desired decomposition products to that of hydrazine. b) Mass spectral profile of released gases over $\text{Cu}@Fe_5Ni_5$ NCs under an argon atmosphere.

in the formation of CuFe_5Ni_5 alloy NPs, as proved by the fact that intraparticle boundaries within a single particle are not observed with HRTEM (SI: Figure S3).

The catalytic reactions were carried out by introducing $\text{N}_2\text{H}_4\cdot\text{H}_2\text{O}$ into the reaction flask containing a catalyst suspension at 70°C in the presence of NaOH. The alkalinity is not only able to convert N_2H_5^+ to N_2H_4 in aqueous solution and to accelerate the rate-determining deprotonation step ($\text{N}_2\text{H}_4 \rightarrow \text{N}_2\text{H}_3^*$)—thus promoting reaction kinetics, but it is also responsible for restraining the generation of the basic by-product NH_3 , increasing the H_2 selectivity of the $\text{N}_2\text{H}_4\cdot\text{H}_2\text{O}$ decomposition.^[7,8] Hence, the addition of NaOH is beneficial for maximally enhancing the catalytic efficacy of the catalysts. **Figure 2a** shows the catalytic activities of the $\text{Cu}@Fe_5Ni_5$ and CuFe_5Ni_5 NCs based on the volume of generated gases. Encouragingly, the $\text{Cu}@Fe_5Ni_5$ NCs exhibit superior catalytic activity and H_2 selectivity—complete release of 3 equivalents of gas only takes 60 min at 70°C . The generated gases were identified by mass spectrometry (MS; **Figure 2b**) to be H_2 and N_2 . To further eliminate the presence of NH_3 , the generated gases are also characterized by gas chromatography (SI: Figure S4), which reveals a $\text{H}_2:\text{N}_2$ ratio of 2.0, in agreement with the volumetric observations, confirming the complete conversion of N_2H_4 to H_2 and N_2 . In contrast, for the CuFe_5Ni_5 NCs, only 2.3 equivalents of gas was generated—even after 125 min under the same reaction conditions. It has been reported that FeNi alloy NCs exhibit 100% H_2 selectivity with a total reaction time of 190 min.^[8] The much superior catalytic activity of $\text{Cu}@Fe_5Ni_5$ relative to CuFe_5Ni_5 and FeNi NCs highlights the significant activity promotion of $\text{Cu}@Fe_5Ni_5$ NCs by introducing a catalytically inactive Cu core, which is derived from the synergistic structural and electronic effects of the metals (via the so-called strain and ligand effects).

As is known to all, the interactions between chemical reactants and the catalyst surface control the activity and efficiency. Precise modification of the catalyst surface at the atomic level and consequently merging the intermetallic electronic interactions is an important pathway for obtaining optimized catalytic performance.^[10b-f] The alloying of Fe and Ni is essential for complete dehydrogenation of N_2H_4 .^[8] Therefore, for CuFe_5Ni_5 NCs, incorporating a third metal component, Cu, with FeNi disturbs the electronic interaction between Fe and Ni on the

catalyst surface, resulting in the degraded catalytic performance. In contrast, for $\text{Cu}@Fe_5Ni_5$ NCs, the introduction of a Cu core does not affect the combined effect of Fe and Ni, but Cu acts as an electron donor for the catalyst surface allowing easier activation of N_2H_4 .^[10] To verify these results, a surface analysis of the $\text{Cu}@Fe_5Ni_5$ NCs was performed by X-ray photoelectron spectroscopy (XPS). The coexistence of the characteristic peaks for Fe 2p and Ni 2p was observed (SI: Figure S5), indicating the lack of segregation. The absence of Cu 2p signals is ascribed to the formation of the $\text{Cu}@Fe_5Ni_5$ core@shell structure. Compared to the standard peaks of Fe and Ni, both of the peaks for Fe $2p_{3/2}$ and Ni $2p_{3/2}$ shift to lower binding energies by ~ 0.4 and ≈ 0.7 eV, respectively, indicating increased electron density in the FeNi surface as a result of the electron-donating effects of Cu. We propose that the synergistic effect between the Cu core and FeNi shell contributes to the high catalytic activity.

Inspired by the electron-donating role of the Cu core, in order to further tune and improve the catalytic performance, a series of $M@Fe_xNi_{(10-x)}$ ($M = \text{Ir}, \text{Pt}, \text{Pd}, \text{Cu}, \text{or Ru}$) NCs with various Fe/Ni molar ratios were prepared via the in-situ seeding-growth approach, and their catalytic performance for the decomposition of $\text{N}_2\text{H}_4\cdot\text{H}_2\text{O}$ were investigated and compared (**Figure 3** and SI: Figure S6). As shown in **Figure 3**, when the shell is composed of both Fe and Ni (regardless of what the core composition is), the H_2 selectivity increases as the Fe/Ni molar ratio increases—with the exception of $\text{Cu}@Fe_9Ni_1$. In contrast, all of the as-synthesized NCs containing a pure Fe shell did not exhibit any activity toward $\text{N}_2\text{H}_4\cdot\text{H}_2\text{O}$ decomposition, which is in agreement with a previous report.^[8] On the other hand, when Ir, Pt, Pd, or Cu was employed as the core and the Fe/Ni molar ratio of the shell was either high or low, i.e., not near 5:5, 100% H_2 selectivity was favored. Comparing the activities of $M@Fe_5Ni_5$, the performance of NCs with noble-metal cores are almost superior to that of NCs with a Cu core (SI: Figure S6). Interestingly, among the investigated $M@Fe_xNi_{(10-x)}$ NCs, the highest catalytic performance is exhibited by the $\text{Pt}@Fe_9Ni_1$ NC, of which a release of 3 equivalents of gas takes only 7 min. However, improved catalytic performance is not observed for the $\text{Ru}@Fe_xNi_{(10-x)}$ NCs, which should be explained by further work.

From the viewpoint of practical application, obtaining 100% H_2 selectivity at decreased temperature is of critical importance. To this end, we tested the catalytic performance of the

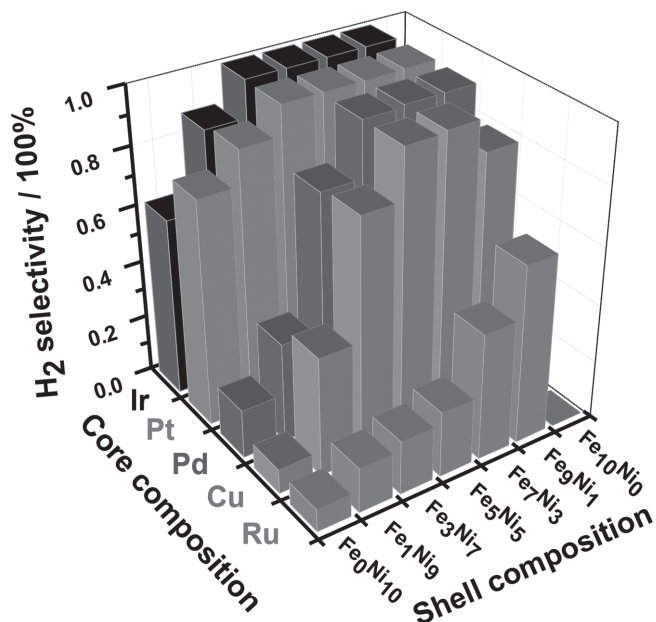


Figure 3. Hydrogen selectivity of the catalytic decomposition of $N_2H_4 \cdot H_2O$ using the as-prepared $M@Fe_5Ni_{(10-x)}$ NCs in the presence of NaOH at 70 °C ($M = Ir, Pt, Pd, Cu$ and Ru ; $x = 0, 1, 3, 5, 7, 9$, and 10).

$Cu@Fe_5Ni_5$ NCs at different temperatures (Figure 4a). When the reaction temperature is decreased to 50 °C, $N_2H_4 \cdot H_2O$ can still be completely converted to H_2 in a reaction time of 250 min. However, upon further decreasing the reaction temperature to 30 °C, 2.1 equivalents of gas can be released from $N_2H_4 \cdot H_2O$ after 21.5 h. Considering the fact that the FeNi alloy NCs only exhibited 100% H_2 selectivity at 70 °C and are inactive at 25 °C,^[8] we can reasonably conclude that the introduction of a Cu core for FeNi active components can effectively reduce the activation energy for the catalytic decomposition of $N_2H_4 \cdot H_2O$, highlighting the synergistic effect of the core@shell structure again. It should be noted that achieving 100% H_2 selectivity from the $N_2H_4 \cdot H_2O$ decomposition at even lower temperature at the cost of decreased activity is extremely worthy from the viewpoint of practical use. Moreover, for $Pt@Fe_5Ni_5$ NCs, 100% H_2 selectivity is obtained with a reaction time of 11 min at 70 °C, 31 min at 50 °C, and 98 min at 30 °C

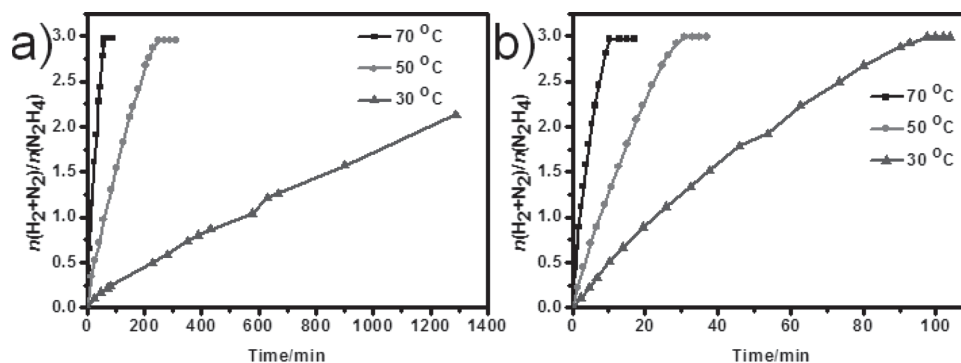


Figure 4. Time-course plots for the decomposition of $N_2H_4 \cdot H_2O$ toward H_2 catalyzed by the $Cu@Fe_5Ni_5$ (a) and $Pt@Fe_5Ni_5$ (b) NCs in the presence of NaOH at different temperatures.

(Figure 4b). Additionally, when 1.5 equivalents of gas is released with the $Cu@Fe_5Ni_5$ and $Pt@Fe_5Ni_5$ NCs, the activation energies were calculated to be 79.2 and 51.2 KJ/mol, respectively.

To investigate the influence of the core content, $Cu_2@Fe_5Ni_5$ and $Pt_{0.5}@Fe_5Ni_5$ NCs were also prepared and applied for the catalytic decomposition of $N_2H_4 \cdot H_2O$. It is found that the activity increases/decreases with the increase/decrease in the amount of the core (SI: Figure S7). In addition, the continuous tests of the catalytic activity revealed good stability of $Cu@Fe_5Ni_5$ NCs (SI: Figure S8).

3. Conclusion

In summary, non-precious-metal-based $Cu@Fe_5Ni_5$ core@shell NCs, prepared via an in-situ seeding-growth approach, not only exhibit good catalytic performance for $N_2H_4 \cdot H_2O$ dehydrogenation at 70 °C, but they also show 100% H_2 selectivity at even lower temperature, highlighting the synergistic effect of core@shell structure. These encouraging findings are certainly helpful for the long-term endeavors in optimizing and enhancing the catalytic efficacy of low-cost catalysts for developing $N_2H_4 \cdot H_2O$ as a viable on-board hydrogen storage material.

4. Experimental Section

Catalyst Preparation: The synthesis of $Cu@Fe_5Ni_5$ NCs follows an in-situ seeding-growth approach. Briefly, $Cu(NO_3)_2 \cdot 3H_2O$ (0.02 mmol), $NiCl_2 \cdot 6H_2O$ (0.1 mmol), $FeSO_4 \cdot 7H_2O$ (0.1 mmol), and PVP (100 mg) were dispersed in 6 mL of H_2O to obtain a transparent solution. Afterwards, the black suspension was obtained by adding an aqueous solution (4 mL) containing NH_3BH_3 (15 mg) with vigorous shaking. The synthesis of $CuFe_5Ni_5$ alloy NCs using $NaBH_4$ (20 mg) instead of NH_3BH_3 as the reducing agent, followed a similar process as that for the $Cu@Fe_5Ni_5$ NCs. For the synthesis of $M@Fe_xNi_{(10-x)}$ NCs ($M = Ir, Pt, Pd, Cu$ or Ru ; $x = 0, 1, 3, 5, 7, 9$ or 10), the amount of M was fixed to be 0.02 mmol whereas the total amount of Fe and Ni was fixed to be 0.2 mmol. A similar process for the $Cu@Fe_5Ni_5$ NCs was used. For the synthesis of $Cu_2@Fe_5Ni_5$ and $Pt_{0.5}@Fe_5Ni_5$ NCs, 0.04 mmol of $Cu(NO_3)_2 \cdot 3H_2O$ and 0.01 mmol of H_2PtCl_6 were used, respectively. Likewise, a similar synthesis as for that of the $Cu@Fe_5Ni_5$ NCs was adopted. NOTE: The complete absence of gas evolution from the solution should be verified before carrying out the tests of the catalytic decomposition of $N_2H_4 \cdot H_2O$.

Characterization: Powder XRD measurements were performed on a Bruker D8 Focus Powder X-ray diffractometer using $Cu K\alpha$

($\lambda = 0.15405$ nm) radiation (40 kV, 40 mA). TEM was performed using a FEI Tecnai G2 S-Twin instrument with a field-emission gun operating at 200 kV. Mass spectrometry analysis of the generated gases was performed using an Ominstar-Thermostar GSD 320 system (Pfeiffer Vacuum) mass spectrometer, wherein argon gas was chosen as the carrying gas. A Techcomp GC7900 gas chromatograph (GC) with a thermal conductivity detector (TCD) was used to analyze the gas products generated from the hydrous hydrazine decomposition. ICP-AES measurements were performed on a TJA (Thermo Jarrell Ash) Atomscan Advantage instrument. XPS measurements were performed on an ESCALAB 250 photoelectron spectrometer.

Catalytic Decomposition of $N_2H_4 \cdot H_2O$: Catalytic reactions were carried out using a two-necked round-bottom flask with one of the flask openings connected to a gas burette and the other for the introduction of $N_2H_4 \cdot H_2O$. The catalytic decomposition reaction of $N_2H_4 \cdot H_2O$ for the release of hydrogen (along with nitrogen) was initiated by shaking the mixture of 2 mmol of $N_2H_4 \cdot H_2O$, which was introduced via a pressure-equalization funnel, and the aqueous suspension of the catalyst prepared as described above in the presence of NaOH (0.1 M). The reaction temperature was kept constant at a specified reaction temperature using a water bath. The gases released during the reaction were passed through a condenser and a trap containing 1.0 M sulfuric acid to ensure the absorption of ammonia, if produced, of which the volume was monitored using the gas burette. To prepare the samples for mass spectral analysis and gas chromatography of the released gases, an acid trap was not used. An illustration of the apparatus for the tests of the catalytic reaction is shown in the SI (Scheme S1).

Supporting Information

Supporting Information is available free of charge from the Wiley Online Library or from the author.

Acknowledgment

This work was financially supported by the fundamental research funds for the central universities, the National Natural Science Foundation of China (Grant No. 51372007 and 213001014).

Received: May 29, 2014

Revised: July 10, 2014

Published online:

- [1] a) L. Schlapbach, A. Züttel, *Nature* **2001**, *414*, 353; b) P. Chen, Z. Xiong, J. Luo, J. Lin, K. L. Tan, *Nature* **2002**, *420*, 302; c) W. Grochala, P. P. Edwards, *Chem. Rev.* **2004**, *104*, 1283.
- [2] a) J. Graetz, *Chem. Soc. Rev.* **2009**, *38*, 73; b) A. W. C. Van de Berg, C. O. Areán, *Chem. Commun.* **2008**, 668; c) U. Eberle, M. Felderhoff, F. Schuth, *Angew. Chem. Int. Ed.* **2009**, *48*, 6608; d) J. Sculley, D. Q. Yuan, H. C. Zhou, *Energy Environ. Sci.* **2011**, *4*, 2721.
- [3] a) E. W. Schmidt, *Hydrazine and its Derivatives: Preparation, Properties, Applications*, 2nd ed., John Wiley & Sons, New York **1984**; b) R. R. Schrock, T. E. Glassman, M. G. Vale, M. Kol, *J. Am. Chem. Soc.* **1993**, *115*, 1760; c) S. H. Wu, D. H. Chen, *J. Colloid Interface Sci.* **2003**, *259*, 282.
- [4] X. Chen, T. Zhang, P. Ying, M. Zheng, W. Wu, L. Xia, T. Li, X. Wang, C. Li, *Chem. Commun.* **2002**, 288.
- [5] a) X. Chen, T. Zhang, M. Zheng, Z. Wu, W. Wu, C. Li, *J. Catal.* **2004**, *224*, 473; b) D. G. Tong, X. L. Zeng, W. Chu, D. Wang, P. Wu, *Mater. Res. Bull.* **2010**, *45*, 442; c) S. K. Singh, X. B. Zhang, Q. Xu, *J. Am. Chem. Soc.* **2009**, *131*, 9894.
- [6] a) S. K. Singh, Q. Xu, *J. Am. Chem. Soc.* **2009**, *131*, 18032; b) S. K. Singh, Q. Xu, *Inorg. Chem.* **2010**, *49*, 6148; c) S. K. Singh, Q. Xu, *Chem. Commun.* **2010**, *46*, 6545; d) S. K. Singh, Z. H. Lu, Q. Xu, *Eur. J. Inorg. Chem.* **2011**, 2232.
- [7] J. Wang, X. B. Zhang, Z. L. Wang, L. M. Wang, Y. Zhang, *Energy Environ. Sci.* **2012**, *5*, 6885.
- [8] S. K. Singh, A. K. Singh, K. Aranishi, Q. Xu, *J. Am. Chem. Soc.* **2011**, *133*, 19638.
- [9] L. He, Y. Huang, A. Wang, X. Wang, X. Chen, J. J. Delgado, T. Zhang, *Angew. Chem. Int. Ed.* **2012**, *51*, 6191.
- [10] a) R. Ghosh Chaudhuri, S. Paria, *Chem. Rev.* **2012**, *112*, 2373; b) D. I. Enache, J. K. Edwards, P. Landon, B. Solsona-Espriu, A. F. Carley, A. A. Herzing, M. Watanabe, C. J. Kiely, D. W. Knight, G. J. Hutchings, *Science* **2006**, *311*, 362; c) S. Alayoglu, A. U. Nilekar, M. Mavrikakis, B. Eichhorn, *Nat. Mater.* **2008**, *7*, 333; d) P. Strasser, S. Koh, T. Anniyev, J. Greeley, K. More, C. F. Yu, Z. C. Liu, S. Kaya, D. Nordlund, H. Ogasawara, M. F. Toney, A. Nilsson, *Nat. Chem.* **2010**, *2*, 454; e) K. Tedsree, T. Li, S. Jones, C. W. A. Chan, K. M. K. Yu, P. A. J. Bagot, E. A. Marquis, G. D. W. Smith, S. C. E. Tsang, *Nat. Nanotechnol.* **2011**, *6*, 302; f) C. J. Serpell, J. Cookson, D. Ozkaya, P. D. Beer, *Nat. Chem.* **2011**, *3*, 478.
- [11] a) J. M. Yan, X. B. Zhang, T. Akita, M. Haruta, Q. Xu, *J. Am. Chem. Soc.* **2010**, *132*, 5326; b) H. L. Jiang, T. Akita, Q. Xu, *Chem. Commun.* **2011**, *47*, 10999; c) H. L. Wang, J. M. Yan, Z. L. Wang, Q. Jiang, *Int. J. Hydrogen Energy* **2012**, *37*, 10229.